In-situ investigation of the anisotropic mechanical behavior of rolled AA 7020-T6 alloy through lattice strain evolution during uniaxial tension

Z. Y. Zhong[1, 2,*], H.-G. Brokmeier[1, 3], E. Maawad[2] and N. Schell[2]

[1]Clausthal University of Technology IWW-TEXMAT, Agricolstraße 6, 38678 Clausthal-Zellerfeld, Germany

[2] Helmholtz-Zentrum Geesthacht, GEMS Outstation at DESY, Notkestraße 85, 22607 Hamburg, Germany

[3] Helmholtz-Zentrum Geesthacht, Max-Planck-Straße 1, 21502 Geesthacht, Germany

Abstract

The texture-induced anisotropic mechanical behavior of a highly textured AA 7020-T6 (maximum orientation density of 29.7 multiple random distribution), was characterized by the lattice strain evolution along rolling direction (RD), 45° to RD and 90° to RD, respectively, under uniaxial tension using high energy X-ray diffraction. The uniaxial tensile tests were done till ultimate tensile strength (UTS), which show different yield strengths (YS), UTS and elongations along the three directions on a macroscopic level. On micromechanical level, the lattice strain evolution explains the correlation between crystallite orientation and different mechanical behavior, leading to the macroscopic anisotropy. In the elastic region, the sample 45° to RD has the lowest lattice plane dependent Young's modulus compared to the other two directions. In the elastic plastic transition region, lattice strain differences among different {hkl} lattice planes are highest for sample 45° to RD and lowest for sample 0° to RD. Moreover, the 45° to RD sample has the lowest lattice dependent YS. In the plastic region, the work hardening behavior of different {hkl} lattice planes in all three directions can be divided into two groups, corresponding to two types of dislocation combinations. However, {200} planes of samples 45° and 90° to RD behave abnormally due to the stress along <110> of the {200} planes and the orientation density of {200} planes parallel and perpendicular to the loading direction (LD).

Keywords: AA 7020-T6 alloy; anisotropy; lattice strain; texture; high energy X-ray diffraction

1. Introduction

Engineering components may exhibit anisotropic mechanical behavior as a function of the angle from the RD due to the producing processes that give rise to preferred orientations, which is considered to be the main contributing factor for the elastic and plastic anisotropy of rolled aluminum alloys [1-3]. The anisotropic mechanical behavior includes different Young's Moduli, yield strengths, UTS and elongations along different directions with respect to RD, which lead to the occurrence of earing during deep drawing of a textured sheet [4]. Literature reported that the 7000 series aluminum alloys have such anisotropic behavior on a macro scale due to texture [5, 6].

---

*Corresponding author. Tel.: +49 040 8998 6906; fax: +49 040 8998 5399.

E-mail address: zhengye.zhong@hzg.de (Z. Y. Zhong).

Postal address: Helmholtz-Zentrum Geesthacht, GEMS Outstation at DESY, Notkestrasse 85, 22607 Hamburg, Germany.

AA 7020 alloy belongs to the 7000 series alloys and is widely used in welded engineering structural components due to the high strength, good weldability and low producing costs. However, AA 7020-T6 exhibits mechanical anisotropy due to the texture resulting from the producing procedures. In industry, the anisotropy is normally characterized by the plastic strain ratio (r-value), which only shows the anisotropic behavior on a macro scale [7]. In contrast, lattice strain evolution reveals that in a textured material, crystallites oriented in a given direction possess specific mechanical behavior, which gives insight into mechanical anisotropy from a micromechanical level.

The lattice strain of individual lattice planes under external load depends on the single crystal properties, on how the lattice planes are oriented with respect to the loading axis and on how they interact with the neighboring crystallites [8]. The first factor belongs to the intrinsic properties of the material, while the last two are extrinsic factors, both of which exert influence on the geometry of dislocation slips. The lattice strain evolutions of face-centered cubic (fcc) materials with random orientations or with weak texture during uniaxial tension were investigated by several researchers [9-15]. In the elastic region, elastic anisotropy, which is expressed by $2C_{44}/(C_{11} - C_{12})$, plays an important role in lattice strain evolution [9, 10, 11]. However, the ratio of Young's moduli E_{111}/E_{200} in a polycrystalline material may be different from that calculated by the Kröner model, because of the interactions with neighboring crystallites, resulting in different lattice plane dependent stress-strain behavior [12]. Furthermore, the measured lattice strains of individual lattice planes imply that the E_{111} is not the largest one in a textured polycrystalline copper, even though the E_{111} is the largest one in copper with random orientations [13]. From elastic-plastic transition region on, lattice strains are dominated by both elastic and plastic anisotropy, the latter of which is dependent on the easiness of dislocation slip. Load redistribution at the elastic-plastic transition region causes lattice strains of different lattice planes to possess different magnitudes. Experimental results show that the lattice planes which yield firstly carry smaller load than the other ones which still deform elastically. For randomly oriented aluminum which has small elastic anisotropy, the crystallites with the normal of {111} planes parallel to LD possess larger lattice strain than the other crystallites, while for copper and stainless steel which have large elastic anisotropy, the crystallites with the normal of {200} planes parallel to the LD possess larger lattice strain [7]. Moreover, the lattice strains of other lattice planes are bounded by those of {111} and {200} lattice planes [9, 10]. Besides, simulation results of lattice strain evolution of weakly textured material can only qualitatively capture the characteristics of the measured results, and Daymond et al. [10] attributed the differences between the simulated results and the measured results to the texture (with maximum orientation density smaller than 3 mrd). By contrast, in the present study, the emphasis is on the lattice plane behavior along different orientations of a highly textured AA 7020-T6 alloy characterized by high energy X-ray diffraction, to understand the mechanisms contributing to the mechanical anisotropy.

Third generation synchrotron radiation provides high-energy X-rays with high brilliance, which makes it possible to get the microstructure information of a material in a short exposure time by transmission technique [16]. It allows *in- situ* lattice strain measurements to be carried out without stopping the loading machine at a relatively low loading speed. During the measurement, complete Debye-Scherrer rings are collected by an area detector, from which one can get the lattice spacing of individual {hkl} lattice planes in both parallel and perpendicular to the LD simultaneously.

2. Experimental

2.1 Material

The investigated material was from a rolled AA 7020-T6 aluminum block with thickness of 29.7 mm. The as-received AA 7020-T6 block, which is used for military use, was got from a French company called CNIM (Constructions industrielles de la Méditerranée) [17]. The AA 7020 block went through T6 heat-treatment (solution heat-treated and artificially aged) after rolling, to get the maximum strength [18]. Its chemical composition of the material is listed in Table 1, which was obtained using atomic emission spectroscopy. Three flat samples were cut from the center layer of as-received AA 7020-T6 block along rolling direction (RD), 45° to RD and 90° to RD, respectively. The sketch of the flat sample is shown in Fig. 1. The thickness of the sample is 3 mm, and the X-ray was parallel to the thickness direction during the measurement. The center layer of the as-received block shows the strong plane-strain rolling texture of high stacking fault energy fcc materials. The orientation distribution function (ODF) analysis results of the center layer are shown in Fig. 2. One can see that the orientations are mainly concentrated along the β fiber which runs from copper component {112}<111> through S component {123}<634> to brass component {011}<211> in Euler space [19]. The maximum orientation density is 29.7 multiple random distribution (mrd). The optical microstructure of the sample exhibits that grains are elongated along RD, as shown in Fig. 3. The sample was etched in the solution consisted of 200 ml distilled water and 5 g 35% tetrafluoroboric acid for 2 minutes under 30 V voltage, which produced different colors on grains with different orientations [20], and the microstructure image was obtained using optical microscopy Olympus-PMG3. The black spots in the Fig. 3 are the precipitates consisting of η', η and T' which were formed after T6 heat-treatment [21].

Table1. Chemical composition of the studied material in weight percent.

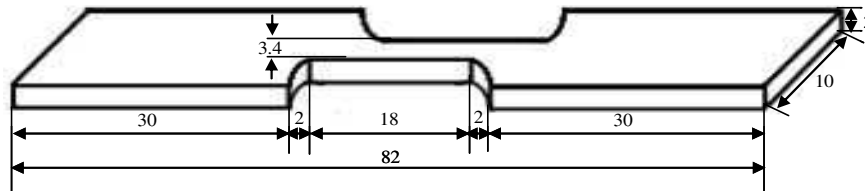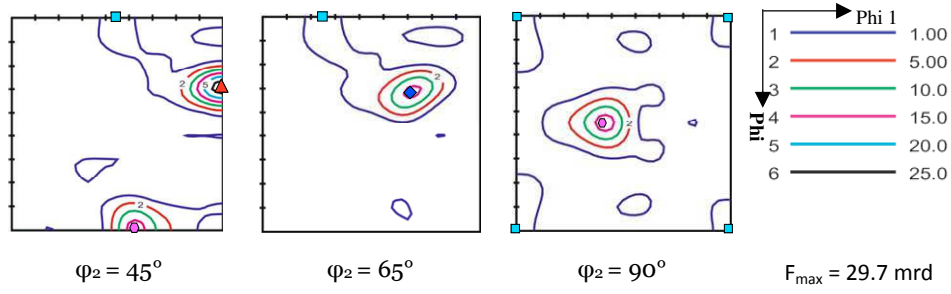|	Zn	Mg	Fe	Mn	Zr	Cu	Si	Ti	Al
AA7020-T6	4.172±0.014	1.215±0.006	0.319±0.009	0.300±0.001	0.148±0.004	0.078±0.001	0.033±0.001	0.013±0.001	Balance

Fig. 1. Sketch of the flat sample (mm).

Fig. 2. The ODF analysis results of the center layer (⬤: Brass component; △: Copper component; ◆: S component; ■: Cube component).
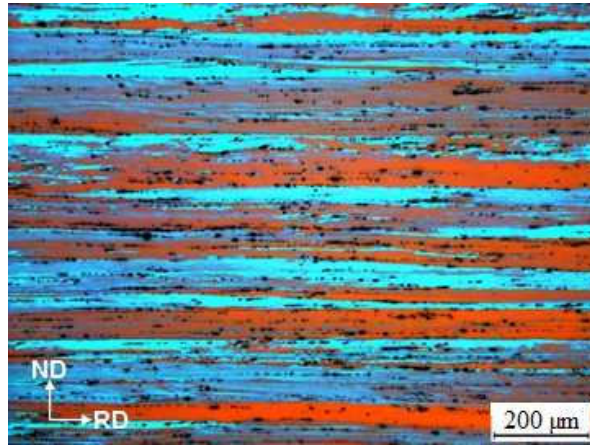

Fig. 3. Microstructure of the sample obtained by optical microscopy.

2.2 Lattice strain measurement

The lattice strain measurements were carried out at the High Energy Material Science beamline HEMS, P07B, at PETRA Ⅲ (DESY, Hamburg). The X-ray beam from the storage ring was monochromatized by a single bounce monochromator (SBM) comprised of two flat water-cooled Laue crystals Si(111) and Si(220), with which the energy can be changed between 53 and 87 keV, respectively. In the present work, the 87 keV X-ray beam (X-ray wavelength of 0.1420 Å) was chosen to characterize the lattice strain evolution with beam size 0.5×0.5 mm^2 and sample-detector distance of 1119 mm. The flat sample was fixed in a universal testing machine (UTM) which can reach the maximum load of 20 kN [22]. The *in- situ* tensile measurements were performed at room temperature with a loading speed of 5×10^{-4} mm/s till UTS. The diffracted beams, Debye-Scherrer rings, were recorded by Perkin Elmer XRD 1622 flat panel, a fast data-collecting area detector which has 2048×2048 pixels with pixel size of 200×200 μm^2. The misalignment of the area detector was corrected by the LaB$_6$ standard powder using the software package FIT2D [23], and the tilting angle of the detector was 0.12°.

The LD of the three samples with respect to the Al (111) pole figure is shown in Fig. 4. *In- situ* tensile tests along these three directions can give insight into the initial texture effects on the lattice strain evolution. The load-elongation curves of the three samples and the measured points are shown in Fig. 5. The elongation is the length change of the whole loading system, which was recorded by the software coupled with the tensile loading machine. The texture dependent yield strengths are 317.8 MPa, 297.5 MPa and 303.5 MPa for the LD parallel to RD, 45° to RD and 90°

to RD samples, respectively. The texture leads to the lowest yield strength in the 45° to RD sample.
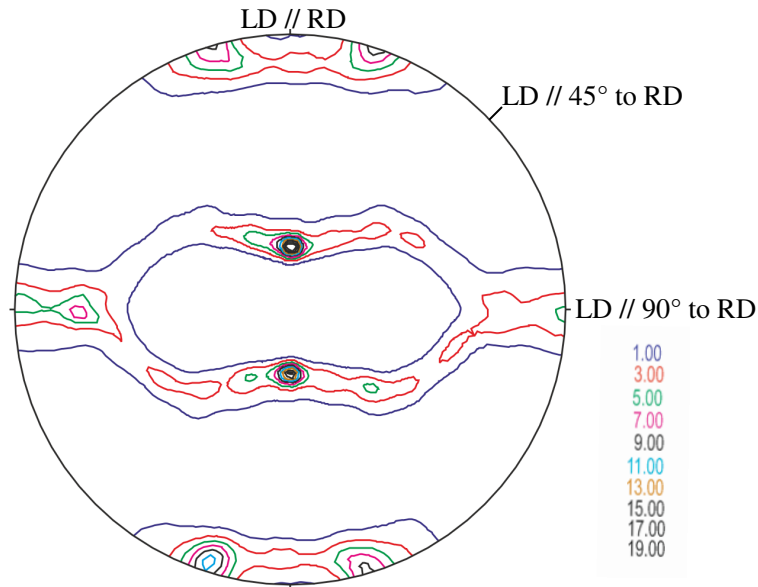

Fig. 4. LD of the three samples with respect to Al (111) pole figure (maximum pole density P_{max} = 24 mrd). The LD of the three samples are parallel to RD, 45° to RD and 90° to RD, respectively.
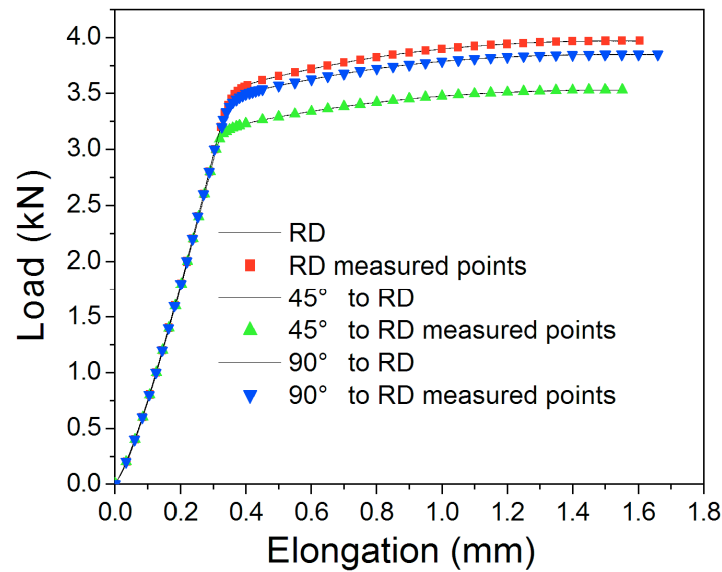

Fig. 5. Load-elongation curves and the measured points.

2.3 Calculating of lattice strain

The diffraction patterns were collected at each measured point shown in Fig. 5. An image from the detector is shown in Fig. 6. The Debye-Scherrer rings correspond to the different {hkl} lattice planes oriented in such a way that they satisfy the Bragg's law with respect to the incident beam. Therefore, it is possible to determine the lattice spacing of particular sets of {hkl} lattice planes which are oriented in certain directions such as LD and perpendicular to LD.

In order to get the lattice spacing of different {hkl} lattice planes oriented along LD and along perpendicular to LD, two sectors along these two directions, respectively, were integrated into a 2θ-intensity spectrum, as shown in Fig. 6. The range of the sector is 10° in γ angle, which means the lattice spacing of specific {hkl} lattice planes is the average value of the crystallites oriented 10° within LD or perpendicular to LD. After that, according to Bragg's equation, 2d * sinθ = λ, one can get the lattice spacing of different {hkl} planes along these two directions. The lattice strain of specific {hkl} lattice planes can be determined from the changes in lattice plane spacing using

$$\varepsilon_{hkl} = \frac{d_{hkl} - d_{0,hkl}}{d_{0,hkl}}$$

where $d_{0,hkl}$ is the lattice spacing of the sample at the beginning of stable elastic deformation [24].
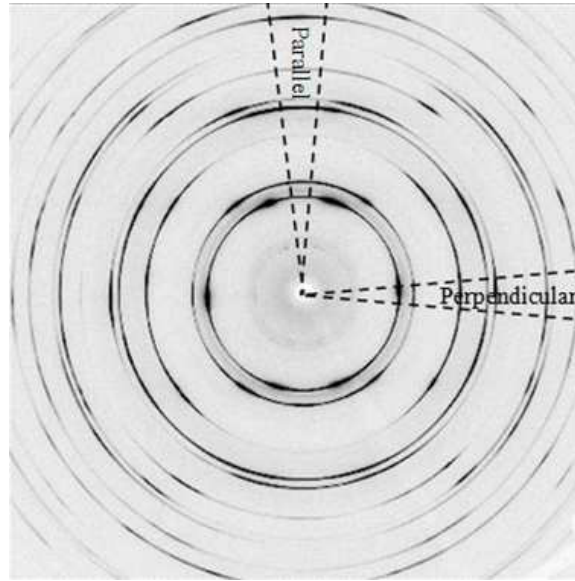

Fig. 6. Integrated sectors along LD and perpendicular to LD (sample LD//RD).

3. Results and discussion

3.1 Overall lattice strain evolution

The texture dependent lattice strain evolutions of different {hkl} lattice planes in both parallel to and perpendicular to the LD are shown in Fig. 7. Due to the strong texture, the intensities of some {hkl} peaks, either in parallel to or perpendicular to the LD, are so low that it is not possible to get the peak positions. Therefore, the lattice strain evolution of some lattice planes may be missing in some of the figures. From Fig. 7, one can see the texture-induced anisotropy through the different responses of individual {hkl} planes oriented in different directions. In the randomly oriented aluminum, the lattice strains of other lattice planes are bounded by those of {111} and {200} lattice planes [9]. However, in the presently investigated samples, the lattice strains of other lattice planes are not bounded by those of {111} and {200} lattice planes due to the strong texture. The behavior of different lattice planes in the 45° and 90° to RD samples are more different than those in the RD sample.
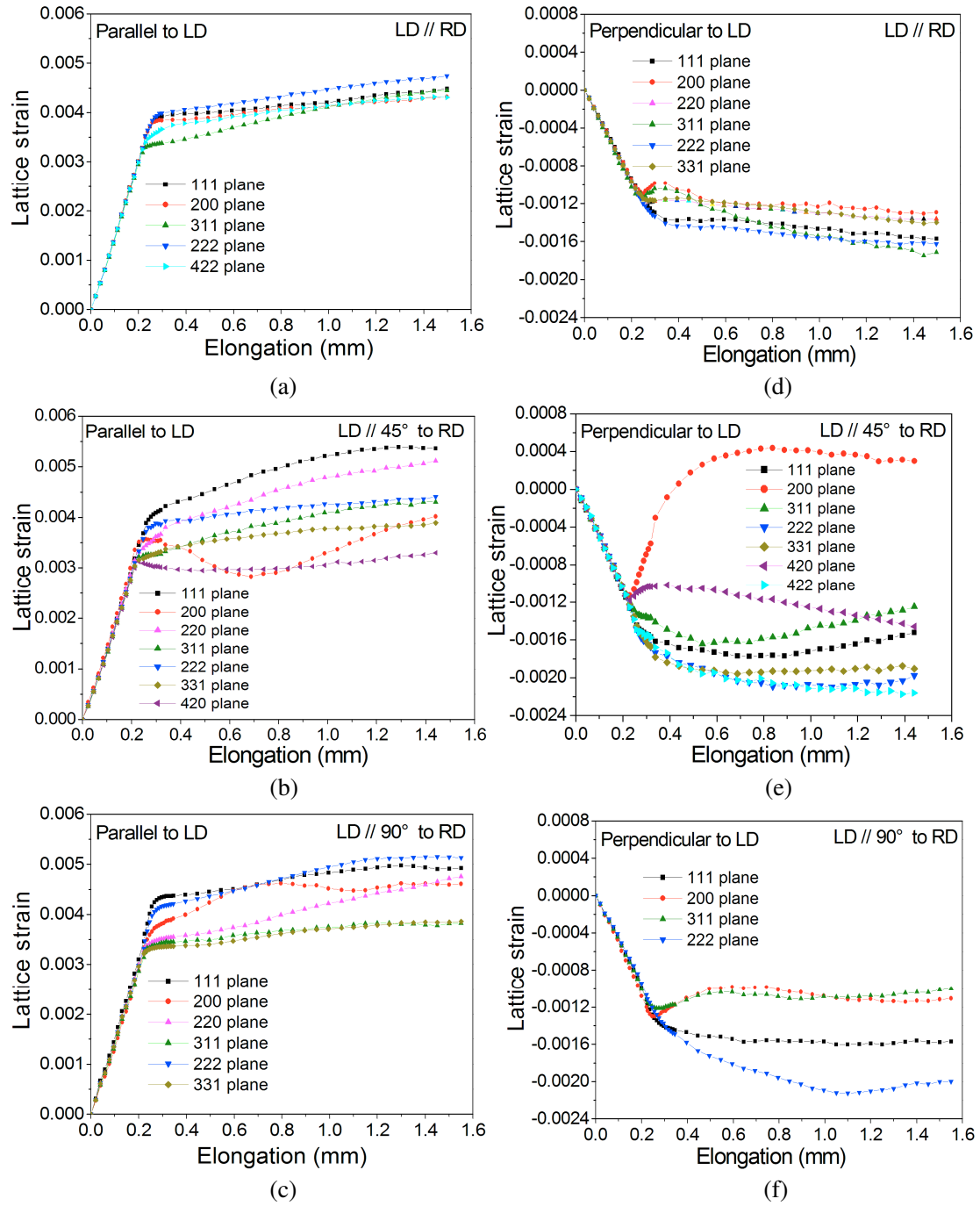
Fig. 7. Lattice strain evolutions of the RD, 45° to RD and 90° to RD samples during uniaxial tension as a function of elongation. (a), (b) and (c) are the lattice strains parallel to LD. (d), (e) and (f) are the lattice strains perpendicular to LD.

3.2 Lattice strain in the elastic region

In the elastic region, parallel to LD, the lattice strains of different {hkl} lattice planes depend on both elastic anisotropy and texture. Since the elastic anisotropy of aluminum is small, which is expressed as $2C_{44}/(C_{11}-C_{12})$ with a value equal to 1.22, the lattice strain differences among different lattice planes are not pronounced, compared to copper and stainless steel which have

higher elastic anisotropy [9]. The magnitudes of the lattice strains of {hkl} lattice planes are influenced by texture, which makes Young's moduli of different lattice planes depend on the orientations with respect to RD. The Young's modulus of a lattice plane can be determined by the slope of the linear fitting of applied stress *vs.* lattice strain in LD ($\Delta\sigma_{//} / \varepsilon_{//,hkl}$), while the Poisson's ratio can be determined using the slope in LD divided by the minus value of the slope in the perpendicular to LD ($-\Delta\sigma_{\perp} / \varepsilon_{\perp,hkl}$), equal to ($-\varepsilon_{\perp,hkl} / \varepsilon_{//,hkl}$). One should notice that the first three points has different slope from the slope of the latter points in elastic region, as shown in Fig. 7 (a), (b) and (c). This is due to the relative movement between the sample and the sample holder, i.e. the elongation of the sample is different from the elongation of the whole loading system at the beginning of the tensile test. Therefore, the latter points in the elastic region are used to calculate the Young's modulus and Poisson's ratio. Fig. 8 shows an example of how to obtain Young's modulus and Poisson's ratio. In Fig. 8 the points used to calculate the Young's modulus and Poisson's ratio are from the 4th to 12th points in Fig. 7 (a). The errors of the Young's modulus and Poisson's ratio are from the error in the elongation, because the lattice strain value is the average value of the whole exposure time, i.e. averaging over a short range of elongation, but in the load-elongation curve, the starting elongation value at the beginning of the exposure time is used to draw a measurement point.

The Young's moduli (E_{hkl}) and Poisson's ratios (ν_{hkl}) of the {hkl} lattice planes of the three samples are shown in Table 2. Owing to the strong texture, the intensities of some reflections in the 2θ spectrum are too low to determine the peak centers either along LD or along perpendicular to LD. Therefore, it is not possible to obtain the corresponding Young's modulus and Poisson's ratio, as shown in the Table 2. As can be seen from the table, the Young's moduli of the lattice planes in the 45° to RD are lower than those in the other two directions. The stiffest reflection {111} in randomly oriented polycrystalline aluminum is no longer the stiffest one in the three measured samples, i.e. the Young's modulus of {111} is not the largest one. Also, the softest reflection {200} in randomly oriented aluminum polycrystalline is not the softest one in the RD and 90° to RD samples. Texture influences the magnitude of lattice strain that a reflection undergoes during uniaxial tension. The magnitude depends on the texture itself, on how the lattice planes are oriented with respect to the LD and on the geometry limitation from the neighboring crystallites. It means that under the same external load, the lattice strains of {hkl} planes in a highly textured material are more limited by the neighboring crystallites than those in a randomly oriented material [25], because in a randomly oriented material different {hkl} lattice planes have equal probability to appear in a given direction. In this case a crystallite oriented in a given direction has equal chance to meet crystallites oriented in other directions. However, in a textured material, a crystallite may have more neighbors with specific orientation. Moreover, the specific orientation correlation between neighboring crystallites may exert influence on the crystallites' behavior [26]. It leads to the measured Young's moduli deviating from those calculated by the Kröner model [25]. For instance, there are very small amounts of {200} planes with their normal parallel to LD in the 90° to RD sample, as shown in Table 3 (The volume fractions of {111} or {200} lattice planes oriented in a given direction were calculated by the software MTEX [27] based on ODF analysis. Here it should be mentioned that for a randomly oriented material, the volume fraction of 10° orientation interval along LD is 19o/ooo. In the present research, the orientations are concentrated on the β fiber [19]. Therefore, the volume fractions listed in the table are smaller than 19o/ooo.). The external load is distributed more to the {111} lattice planes,

making the lattice strain of {200} smaller than that of {111}. It causes the measured Young's modulus of the {200} to be larger than that of {111} in this sample.
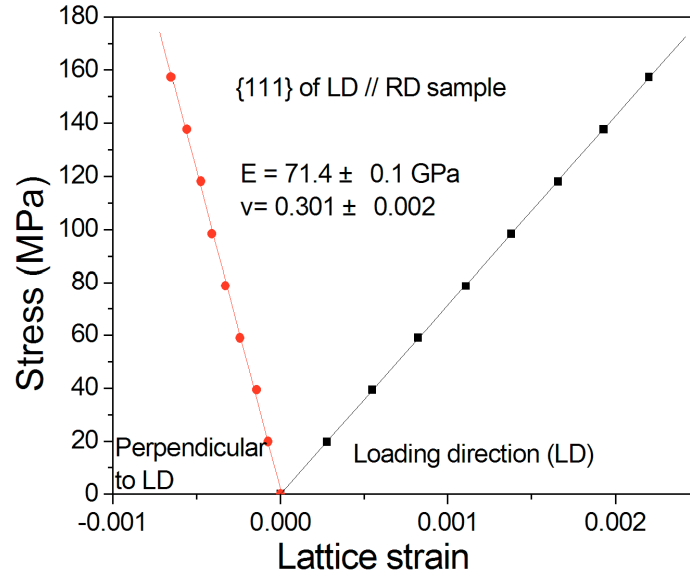

Fig. 8. An example of determining the Young's modulus and Poisson's ratio.

Table 2. Young's modulus, Poisson's ratio and yield strength of different lattice planes.

Lattice plane	200	311	420	422	220	331	111
LD parallel to RD							
E_{hkl}/GPa	71.5±0.2	73.3±0.3	---	72.3±0.3	---	---	71.4±0.1
ν_{hkl}	0.298±0.004	0.322±0.003	---	---	---	---	0.301±0.002
YS/MPa	314.1	312.3	---	322.2	---	---	315.4
LD parallel to 45° to RD							
E_{hkl}/GPa	64.8±0.9	70.0±0.3	71.3±0.2	---	67.8±0.1	70.9±0.1	66.9±0.5
ν_{hkl}	0.338±0.007	0.362±0.006	0.374±0.004	---	0.332±0.004	0.368±0.002	0.355±0.006
YS/MPa	290.2	296.1	299.8	---	298.6	304.7	293.6
LD parallel to 90° to RD							
E_{hkl}/GPa	73.1±0.7	75.2±0.7	---	---	71.7±0.7	72.8±0.7	70.6±0.7
ν_{hkl}	0.368±0.009	0.349±0.007	---	---	---	---	0.323±0.006
YS/MPa	295.8	311.4	---	---	312.7	308.8	298.5
Values calculated by the Kröner model for random aluminum polycrystalline							
E_{hkl}/GPa	66.7	69.2	69.3	70.8	70.8	71.2	72.3
ν_{hkl}	0.358	0.352	0.352	0.349	0.349	0.348	0.346

	Macroscopic yield strength		
	LD parallel to RD	LD parallel to 45° to RD	LD parallel to 90° to RD
YS/MPa	317.8	297.5	303.5

Table 3. The amounts of crystallites with the normal of {111} and {200} parallel or perpendicular to the LD (volume fraction ‰).

Samples	LD// RD	LD//45° to RD	LD//90° to RD
Crystallites with the normal of {111} parallel to the LD	14.7	2.5	17.2
Crystallites with the normal of {200} parallel to the LD	3.1	5.0	0.7
Crystallites with the normal of {111} perpendicular to the LD	17.2	2.8	14.7
Crystallites with the normal of {200} perpendicular to the LD	0.7	8.4	3.1

3.3 Lattice strain in the elastic plastic transition region

When it approaches the elastic plastic transition region, anisotropic behavior of individual lattice planes oriented in different directions with respect to the rolling coordinates can be directly observed, which gives a hint of the texture-induced anisotropy. The lattice strain differences among different {hkl} lattice planes are larger in the 45° and 90° to RD samples than those in the RD sample, indicative of a more diverse load redistribution, as shown in Fig. 7 (a) to (c).

Parallel to LD, in the RD sample, the lattice strain of {311} inflects while the lattice strains of {111}, {222} and {200} still increases linearly, indicating that in this sample the {111}, {222} and {200} are the lattice planes which carry more load in the elastic plastic transition region. Similarly, in the 45° to RD sample, {111} and {222} carry more load than {311}, {331} and {420}, and in the 90° to RD sample, {111} and {222} carry more load than {220}, {311} and {331}. All the other lattice planes appeared in Fig. 7 (a) to (c) but not mentioned above, carry loads that are between maximum and minimum. In contrast, in the aluminum with random orientations, the {111} carries the highest load and the {200} carries the lowest load in the elastic plastic transition region [28]. Therefore, the lattice strain behavior shows that load redistribution in the elastic plastic transition region is texture-dependent. However, the {111} lattice planes are the main load carrier in all three samples. Perpendicular to LD, the lattice strains of different lattice planes are controlled by Poisson contraction and interaction between neighboring crystallites, which will be more discussed in the section 3.4.

The yield strength of individual lattice planes can be determined from the stress-lattice strain plot. The stress value where the lattice strain starts to deviate from linearity is defined as the yield strength. The yield strengths of individual {hkl} lattice planes in different directions are shown in Table 2. The {hkl} lattice planes of the 45° to RD sample have the lowest yield strengths among the three samples, which reveal the reason why the macro yield strength of this sample is the lowest. Texture changes the dislocation slip geometry which is determined by both the orientations of the {hkl} lattice planes with respect to the LD and the orientations between {hkl} lattice planes and their neighboring crystallites. This leads to a larger resolved shear stress in the 45° to RD [29]. It results in the lower lattice plane dependent yield strength in this direction.

3.4 Lattice strain in the plastic region

In the plastic region, the differences of stress-strain response among {hkl} lattice planes are more evident than in the elastic region, depending on the initial texture, as shown in Fig. 7. However, in this region parallel to LD, except the abnormal behavior of the {200} lattice planes, work hardening behavior can be mainly divided into two groups, which is deduced from the slope

of the lattice strain *vs.* elongation curve, as shown in Fig. 7 (a)-(c). The first group shows a very small strain hardening rate, e.g. the {222} and {420} in the 45° to RD sample, as shown in Fig. 7 (b). The second group shows an increasing lattice strain curve. The slope of the lattice planes in this group is almost the same, e.g. the {111}, {220} and {311} in the 45° to RD sample. The work hardening behavior of the other lattice planes which do not belong to these two groups show intermediate situation between the two groups. When it gets close to UTS, the work hardening behavior of almost all lattice planes becomes similar, which may be attributed to the dislocation density inside the material. In our other study, we found that dislocation multiplication and annihilation became balanced with each other in this region [30].

The two types of the work hardening behavior can be attributed to the stress states which the individual lattice planes undergo. Bishop established that four different types of crystallographic stress states can activate polyslip [31], and Kocks investigated the work hardening behavior of the different types of polyslip [32]. Based on their results, the two work hardening behavior are caused by the so called [100] tension and [111] tension stress states, respectively. The [100] tension stress state activates 8 slip systems. The combination of these 8 slip systems cannot make contributions to the hardening on the effected lattice planes. By contrast, the [111] tension stress state activates 6 slip systems, but it can harden the effected lattice planes. Those lattice planes whose strain hardening behavior are between the two groups are in the stress state which is in the combination of the [100] tension and [111] tension.

The abnormal behavior of {200} lattice planes are attributed to two factors. One is the amount of crystallites with the normal of {200} lattice planes parallel or perpendicular to the LD, i.e. texture, which are shown in Table 3. The other one is whether the <110> directions of the {200} planes are stressed or not, depending on the interactions between neighboring crystallites. When the <011> directions of the {200} planes are stressed, the active slip systems are (111)[10-1], (111)[01-1], (11-1)[101] and (11-1)[011]. If the amount of slip on the 4 active slip systems is the same, the deformation is asymmetric. It will cause large contraction in the [001] direction [28, 33]. If the contraction is along the LD, it will cause tensile stress to the {200} lattice planes, as shown in Fig. 7 (c). If the contraction is opposite the LD, it will cause a compressive stress to the {200} lattice planes, as shown in Fig. 7 (b). However, as the deformations goes on, the lattice planes rotates in such way that the <110> directions of the {200} planes are not stressed, resulting in the decrease of the contraction along the [001] direction.

Perpendicular to the LD, the lattice strain evolution after yield is mainly controlled by the Poisson contraction and the interaction among neighboring crystallites, the latter of which is strongly related to the texture. The effect of the interaction among neighboring crystallites can be demonstrated by lattice strain evolution differences of the {111} and {222} lattice planes, as shown in Fig. 7 (e) and (f). The reason for this is that the difference of the 2θ values for {111} and {222} is around 3.5° under the experimental condition, which means that {111} and {222} planes are from two different groups of grains (with 1.74° difference in the orientation). The different groups of grains may have different neighboring grains having different orientations, i.e. the orientation correlations [26] with the neighboring grains are different, which may lead to the different lattice behavior of the {111} and {222}. However, further investigation on this point via numerical simulation is required. The lattice strain of {200} in the 45° to RD sample shows positive values, which indicates that both the <110> directions of {200} are stressed and there are sufficient amounts of crystallites with the normal of {200} perpendicular to the LD, as shown in

Fig. 7 (e) and Table 3. Under this condition, the contraction along the [001] direction can offset the Poisson contraction. However, in the RD and 90° to RD samples, there are not enough such crystallites so that the lattice strain of {200} only experiences a tensile stress at the beginning of this region, as shown in Fig. 7 (d) and (f).

4. Conclusion

The lattice strain evolution along the three directions, i.e. RD, 45° to RD and 90° to RD of a highly textured AA 7020-T6 alloy shows that the lattice-dependent Young's moduli, yield strengths, the amount of {hkl} lattice planes oriented in a given direction and the interactions with the neighboring crystallites, lead to the macroscopic anisotropy which exhibits the lowest yield strength and UTS along the 45° to RD and highest along RD. In the elastic region, the texture-dependent lattice strain evolution indicates that the Young's moduli of the lattice planes with normal along 45° to RD have the smallest values. Furthermore, the deviations of the measured Young's moduli from those calculated by the Kröner model for polycrystalline aluminum with random orientations, are related to the amount of {hkl} lattice planes in a specific direction and the deforming limits from the neighboring crystallites.

In the elastic plastic transition region, the load redistributions in the 45° and 90° to RD samples are more diverse than those in RD sample. The texture changes the dislocation slip geometry along different directions with respect RD, making the lattice plane dependent yield strength along 45° to RD the one with the lowest value.

In the plastic region, parallel to LD, the so-called [100] tension and [111] tension stress states are dominant in all the three samples, resulting in two types of strain hardening behavior. The abnormal behavior of {200} lattice planes is related to whether the <110> directions of {200} are stressed, which induces a contraction along the [001] direction. If the contraction along the [001] direction is parallel to the LD, it will induce a tensile stress along LD. If the contraction along the [001] direction is opposite to the LD, it will induce a compressive stress along LD. Perpendicular to LD, the lattice strain of individual lattice planes are controlled by the Poisson contraction and the interactions among the neighboring crystallites. The {200} lattice planes of the 45° to RD sample exhibit positive lattice strains due to both the contraction along the [001] directions of {200} lattice planes and the amount of {200} lattice planes, which are strongly related to the initial texture.

Acknowledgements

References

[1] O. Engler, Y.G. An, Solid State Phenom. 105 (2005) 973-997.
[2] M.A. Zaidi, T. Sheppard, Mater. Sci. Technol. 1 (1985) 593-559.

[3] P.S. Bate, Y.G. An, Scr. Mater. 51 (2004) 973-997.

[4] O. Engler, J. Hirsch, Mat. Sci. Eng. A 452 (2007) 640-651.

[5] D. Achani, O.S. Hopperstad, O.G. Lademo, J. Mater. Process. Technol.209 (2009) 4750-4764.

[6] C. Mondal, A.K. Singh, A.K. Mukhopadhyay, K. Chattopadhyay, Mater. Sci. Forum 702-703 (2012) 303-306.

[7] O. Engler, Y.G. An, Solid State Phenom. 105 (2005) 277-284.

[8] A.M. Korsunsky, M.R. Daymond, K.E. James, Mat. Sci. Eng. A 334 (2002) 41-48.

[9] B. Clausen, T. Lorentzen, T. Leffers, Acta Mater. 46 (1998) 3087-3098.

[10] M.R. Daymond, C.N. Tomé, M.A.M. Bourke, Acta Mater. 48 (2000) 553-564.

[11] B. Clausen, M.A.M. Bourke, Metall. Mater. Trans. A, 32A (2001) 691-694.

[12] P. Dawson, D. Boyce, S. MacEwen, R. Rogge, Mat. Sci. Eng. A 313 (2001) 123-144.

[13] C.J. Neil, J.A. Wollmershauser, B. Clausen, C.N. Tomé, S.R. Agnew, Int. J. Plast. 26 (2010) 1772-1791.

[14] B. Clausen, T. Lorentzen, M.A.M. Bourke, M.R. Daymond, Mat. Sci. Eng. A 259 (1999) 17-24.

[15] J.W.L. Pang, T.M. Holden, T.E. Mason, Acta Mater. 46 (1998) 1503-1518.

[16] M.R. Daymond, P.J. Withers, Scripta Mater. 35 (1996) 1229-1234.

[17] http://www.cnim.com/.

[18] R. Howard, N. Bogh, D.S. MacKenzie, in: G.E.Totten, D.S. MacKenzie (Eds.), Handbook of Aluminum: Volume 1: Physical Metallurgy and Processes, Marcel Dekker, Inc. New York, 2003, pp. 881-970.

[19] J. Hirsch, K. Lücke, Acta Metall. 36 (1988) 2883-2904.

[20] G.F. Vander Voort, Metallography: Principles and Practice, McGraw-Hill, New York, 1984.

[21] L. Katgerman, D. Eskin, in: G.E.Totten, D.S. MacKenzie (Eds.), Handbook of Aluminum: Volume 1: Physical Metallurgy and Processes, Marcel Dekker, Inc. New York, 2003, pp. 259-303.

[22] S.-B. Yi, C. Davies, H.-G. Brokmeier, R. Bolmaro, K. Kainer, J. Homeyer, Acta Mater. 54 (2006) 549-562.

[23] A.P. Hammersley, S.O. Svensson, A. Thompson, Nucl. Instrum. Methods A, 346 (1994) 312-321.

[24]. E. Maawad, H.-G. Brokmeier, Z.Y. Zhong, N. Al-Hamdany, M. Salih, N. Schell, Mat. Sci. Eng. A 594 (2014) 62-67.

[25] M. Kamaya, Int. J. Solids Struct. 46 (2009) 2463-2649.

[26] H.J. Bunge, in: H.R. Wenk (ed.), Preferred Orientation in Deformed Metals and Rocks: An Introduction to Modern Texture Analysis, Academic Press, Inc. Orlando, 1985, pp. 507-526.

[27] F. Bachmann, R. Hielscher, H. Schaeben, Solid State Phenom. 160 (2010) 63-68.

[28] B. Clausen, Ph.D. thesis (Risø-R-985(EN) thesis), Risø National Laboratory, Denmark, 1997.

[29] N.S. Lee, J.H. Chen, P.W. Kao, L.W. Chang, T.Y. Tseng, J.R. Su, Scr. Mater. 60 (2009) 340-343.

[30] Z.Y. Zhong, H.-G. Brokmeier, W.M. Gan, E. Maawad, B. Schwebke, N. Schell, Mater. Charact., under review.

[31] J.F.W. Bishop, Phil. Mag. 44 (1953) 51-64.

[32] U.F. Kocks, Acta Metall. 8 (1960) 345-352.

[33] W.F. Hosford, Trans. Met. Soc. AIME 230 (1964) 12-15.